A Novel Trapezoidal Wave Control Method for a Single-Phase Grid-Tied T-Type Inverter

Zhen Zhang, Junming Zhang, *Senior Member, IEEE*, and Shuai Shao, *Member, IEEE*

***Abstract*—Triangular conduction mode (TCM) is used in grid-tied inverters to achieve high efficiency by its soft switching feature. However, it suffers from a wide switching frequency variation over the whole power range, which impacts the weighted efficiency. To address this issue, this article proposes a novel trapezoidal wave control method for a single-phase grid-tied T-type inverter. By the proposed method, the inductor current is divided into three stages in a switching cycle, so it looks like trapezoidal wave rather than triangular wave. The proposed trapezoidal wave has two independent conduction times. In order to simplify the control, the proportion between the two conduction times is controlled as a variable. As a result, only one conduction time needs to be calculated, and the derived equation is easy to be calculated in digital controllers. Furthermore, this article proposes a design consideration for the value selection of the proportion between the two conduction times, which ensures proper operation of the circuit. The proposed scheme has three advantages. First, it realizes soft switching in every switching cycle. Second, it reduces the switching frequency and related losses compared to the full-bridge inverter in TCM operation and thus improves efficiency. Third, it can be applied over the whole line cycle as a uniform operation mode. Therefore, mode transitions are avoided, which improves the quality of the grid-injected current. A prototype has been built and the experimental results verify the feasibility of the proposed scheme.**

***Index Terms*—Boundary conduction mode, soft switching, triangular conduction mode, T-type inverter.**

I. Introduction

SINGLE-PHASE grid-tied inverters with low-and-medium power levels and unity power factor have been widely used in photovoltaic systems [1], [2]. Besides the basic requirements, such as performance, reliability, and cost, high efficiency is also an important indicator for inverters. One of the most researched techniques to improve the inverter's efficiency is soft switching technique [3]–[5]. However, most of them require auxiliary circuits, which increase control complexity and system cost. Besides that, multilevel techniques, which are mainly used in medium-and-high voltage applications, are nowadays more and more used in low-voltage and low-power applications [6]–[13]. This is because it can decrease the switching frequency and related losses with the inductor current ripple unchanged. Also, wide band gap (WBG) semiconductor device is an alternative to traditional ones, which could increase efficiency without changing circuit topology and control method. However, silicon devices are still mainstream in the market and it still needs more efforts to improve the WBG device reliability and drive down the cost.

In recent research works, boundary conduction mode (BCM) is more and more adopted in low-voltage, low-and-medium power grid-tied inverters to reduce the inductor size and achieve soft switching without extra circuits [16]–[28].

The BCM operation can be divided into two types according to the operation principle, i.e., critical conduction mode (CRM) [14] and triangular conduction mode (TCM) [15]. For the CRM operation, the switching cycle is restarted when the inductor current reaches zero. Valley switching (VS) is achieved by the resonance between the inductor and the output capacitor of transistors. The CRM operation is usually used for flyback inverters [16]–[17]. On the other hand, for the TCM operation, the switching cycle is restarted when the inductor current is driven to a small negative boundary instead of zero [15]. With the help of the reverse inductor current, the charge in the output capacitor of the main transistor is recycled to the dc voltage source and zero voltage switching (ZVS) is guaranteed in each switching cycle. The TCM operation has been used in several topologies, such as single-phase full-bridge inverter [18], three-phase half-bridge inverter [19], three-phase half-bridge T-type inverter [20], and single-phase hybrid-bridge T-type inverter [21].

The main disadvantage of BCM operation is a wide switching frequency variation over the whole power range. Therefore, the weighted efficiency is deteriorated. To address this issue, researchers use multimode control to optimize the efficiency. The core idea is to apply different operation modes for different instantaneous power. For example, the works in [22]–[25] combine CRM and DCM (discontinuous conduction mode) operations together in a half line cycle to improve the overall efficiency. As the instantaneous power exceeds a threshold, the inverter operates in CRM and this can limit the peak current amplitude and the conduction losses. As the instantaneous power drops below the threshold, the inverter operates in DCM and this can avoid ultrahigh switching frequency and related switching losses. The works in [26]–[28] adopt a similar method, which is called dual-mode control. In this case, the inverter always operates in TCM operation, and the

Manuscript received January 16, 2020; revised April 2, 2020, May 29, 2020, and August 13, 2020; accepted September 11, 2020. Date of publication September 22, 2020; date of current version November 20, 2020. This work was supported by the National Natural Science Foundation of China under Grant 51877193 Recommended for publication by Associate Editor J. Biela. *(Corresponding author: Junming Zhang.)*

The authors are with the College of Electrical Engineering, Zhejiang University, Hangzhou 310027, China (e-mail: zhang_zhen@zju.edu.cn; zhangjm@zju.edu.cn; shaos@zju.edu.cn).

Color versions of one or more of the figures in this article are available online at https://ieeexplore.ieee.org.

Digital Object Identifier 10.1109/TPEL.2020.3025965

reverse boundary of the inductor current is designed to different values for two zones. The large reverse boundary could decrease the switching frequency and is suitable for low instantaneous power. The small reverse boundary could decrease peak current and is suitable for high instantaneous power. Another way to reduce the switching frequency variation range is to use the multilevel topology. Usually, multilevel topologies operate in fixed frequency continuous conduction mode. Zhang *et al.* [21] propose a single-phase hybrid-bridge T-type inverter in TCM operation in order to narrow the switching frequency range and reduce related losses. However, the inverter has to switch to full-bridge operation when the output voltage is close to half of the dc input voltage to avoid extreme low switching frequency, and the quality of the grid-injected current would be affected because of mode transitions in a line cycle. Therefore, further improvement is still necessary.

This article proposes a novel trapezoidal wave control method based on the single-phase hybrid-bridge T-type inverter, which can be seen as an improvement of literature [21]. With the proposed method, the inductor current is divided into three stages in a switching cycle, so it looks like trapezoidal wave rather than triangular wave. The proposed scheme has three advantages. First, it achieves soft switching in every switching cycle. Second, it reduces the switching frequency and related losses compared to the full-bridge inverter in TCM operation and thus improves efficiency. Third, it can be applied over the whole line cycle as a uniform operation mode. So mode transitions are avoided, which improves the quality of the grid-injected current.

The proposed trapezoidal wave has two independent conduction times. So the related calculation becomes flexible and complicated. In order to simplify the control and save computation resources, the proportion between the two independent conduction times is controlled as a variable. As a result, only one conduction time needs to be calculated. Moreover, based on the proposed constraint, the derived equation for the conduction time calculation becomes simple and easy to be executed in digital controllers.

The proportion between the two conduction times affects the shape of the trapezoidal inductor current and its value selection is flexible. Therefore, this article proposes a value selection strategy for the proportion between the two conduction times. It not only ensures the normal operation of the circuit, but also optimizes the proposed scheme.

The remainder of this article is organized as follows. Section II discusses the principle of the proposed trapezoidal wave control method, Section III discusses a strategy for the value selection of the proportion between the two conduction times, Section IV discusses the prototype design and experimental results. Finally, Section V draws the conclusion.

II. Principle of the Proposed Trapezoidal Wave Control Method

The proposed trapezoidal wave control method is suitable for hybrid-bridge T-type inverter, as shown in Fig. 1. The T-type leg operates at high frequency (HF) to modulate a sinusoidal output current and the two-level leg operates at line frequency (LF) as an unfolder. The T-type leg could also be replaced by diode-clamped leg and flying-capacitor leg. In this article, the T-type leg is used because of its low conduction losses and simplicity in control.

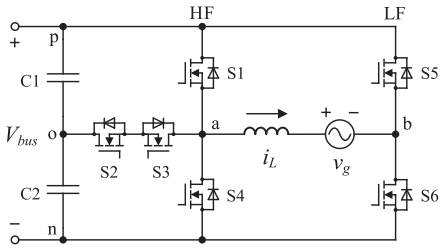

Fig. 1. Topology of the hybrid-bridge T-type inverter.

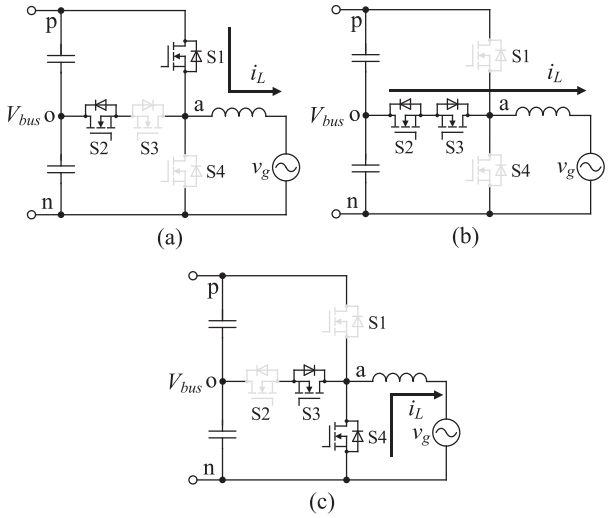

Fig. 2. Three operation stages of the circuit with the proposed trapezoidal wave in a switching cycle during the positive half line. (a) Stage 1. (b) Stage 2. (c) Stage 3.

Fig. 2 shows the three operation stages of the circuit with the proposed trapezoidal wave control method in a switching cycle during the positive half line. Digital signal processor (DSP) is used to control the whole system and its built-in ePWM module is used to control the switches. In order to make the control of the T-type leg compatible with the configuration of ePWM module, S1 and S3 are assigned to a set of ePWM module and operate in a complementary way. S2 and S4 are assigned to a set of ePWM module and operate in a complementary way too.

Fig. 3 shows the related key waveforms of the proposed method. The time counters of the two ePWM modules are synchronized. S1 and S2 are controlled as active switches, since S1 and S3 are complementary, S2 and S4 are complementary. COMP A and COMP B are two parameters in the ePWM module, which are compared with the time counter to generate switching actions. COMP A determines the action of S1 & S3 and the conduction time (T1) of the first stage, and COMP B determines the action of S2 & S4 and the conduction time (T2) of the second stage. k_1, k_2, and k_3 represent the slope of the inductor current, T_1, T_2, and T_3 represent the conduction

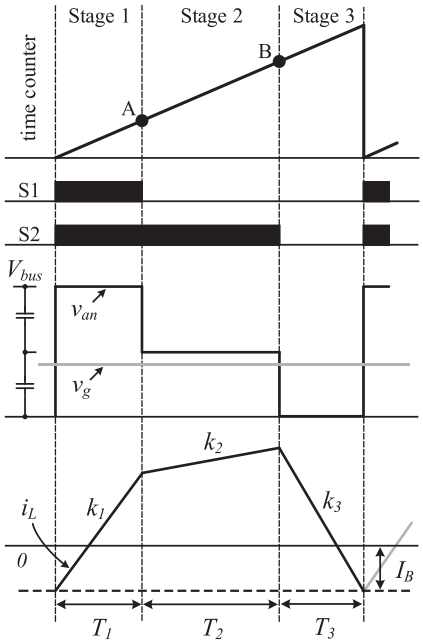

Fig. 3. Key waveforms of the proposed trapezoidal wave in a switching cycle during the positive half line.

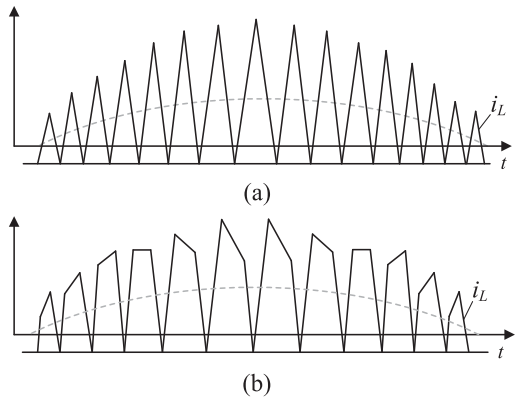

Fig. 4. Inductor current over a half line cycle. (a) TCM operation. (b) Proposed trapezoidal operation.

time of the three stages, and IB represents the reverse boundary of the inductor current. Once the inductor current reaches the reverse boundary, a new switching cycle is started. The operation principle is detailed as follows.

A. Stage 1

The equivalent circuit is shown in Fig. 2(a). In the beginning of a switching cycle, the time counter equals 0 and S1 and S2 are turned ON simultaneously. At this time, the current flows through S1 automatically. As a result, the output of the T-type leg is connected to the positive dc bus terminal. The voltage across the inductor equals $V_{\rm bus} - v_g$ and the inductor current increases linearly from the reverse boundary.

B. Stage 2

The equivalent circuit is shown in Fig. 2(b). When the time counter reaches COMP A, S1 is turned OFF and S3 is turned ON. At this time, the current flows through S2 and S3. The output of the T-type leg is connected to the midpoint of the dc bus and the voltage across the inductor equals $V_{\rm bus}/2–v_g$. In this stage, if v_g is lower than $V_{\rm bus}/2$, the inductor current slope (k_2) is positive, and if v_g is higher than $V_{\rm bus}/2$, the inductor current slope is negative. If v_g equals $V_{\rm bus}/2$, the inductor current would freewheel with zero slope.

C. Stage 3

The equivalent circuit is shown in Fig. 2(c). When the time counter rises to COMP B, S2 is turned OFF and S4 is turned ON. At this time, the current flows through S4. The output of the T-type leg is connected to the ground. The voltage across the inductor equals $-v_g$ and the inductor current decreases linearly to the reverse boundary again.

Fig. 4 shows the inductor current of the TCM operation and the proposed trapezoidal operation over a half line cycle. The current waveform by the proposed scheme is different from the conventional triangular waveform, while the average current is the same.

The proposed trapezoidal wave control method has several advantages. First, soft switching is realized in each switching cycle by the proposed scheme. In stage 3, as shown in Fig. 2(c), S3 and S4 are ON, and the inductor current freewheels through S4. The voltage across S1 and S2 is bus voltage and half of the bus voltage, respectively, whereas the voltage across S3 and S4 is zero. At the end of stage 3, the inductor current reverses and increases through S4 toward the negative boundary, as shown in Fig. 3. Once the inductor current reaches the negative boundary, the next switching cycle is started. At this time, S4 and S3 are turned OFF first, and after a dead time, S1 and S2 are turned ON. During the dead time, soft switching is realized, as shown in Fig. 5. The reversed inductor current would charge the output capacitors of S3 and S4, and at the same time discharge the output capacitors of S1 and S2. Therefore, the voltage across S1 and S2 drops and the voltage across S3 and S4 rises. Finally, the transient resonance ends and the inductor current flows through the body diode of S1. This creates a zero-voltage turn-ON condition for S1. From another point, the charge stored in S1 and S2 is recycled to the dc bus rather than dissipated in the circuit.

The second advantage of the proposed scheme is that it can decrease the switching frequency and related losses compared to the full-bridge inverter in TCM operation with the same inductor. In fact, when the inductor is the same and the average inductor current is the same, the switching period or frequency is related to the slope of the inductor current, or we can say is related to the voltage across the inductor. For the full-bridge inverter in TCM operation, the voltage across the inductor is large; so, in a switching cycle, the inductor current rises and drops in a large slew rate and the switching period is short. For the proposed scheme, although it has three stages in a switching cycle, at least at one stage, the voltage across the inductor is relatively small. So the inductor current changes slowly and the

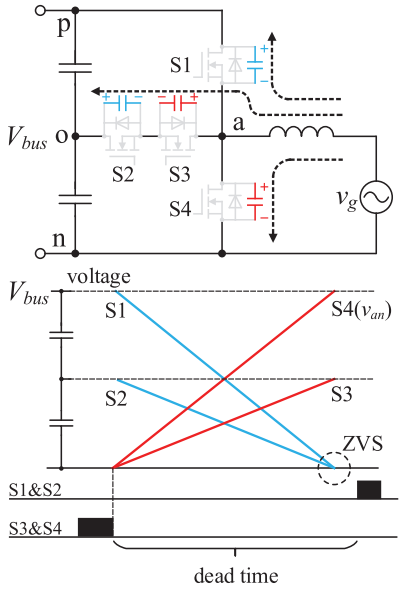

Fig. 5. Soft switching principle of the trapezoidal wave control method.

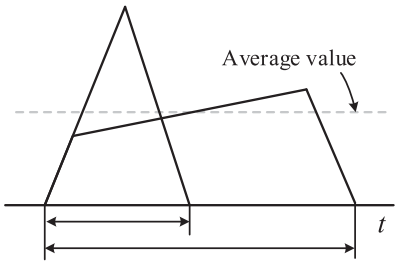

Fig. 6. Switching period is lengthened by the proposed trapezoidal wave control method.

switching period is lengthened. Fig. 6 illustrates this feature. On the other hand, when the switching frequency range is kept at the same level, the proposed scheme allows the use of smaller inductors compared to the full-bridge inverter in TCM operation.

The third advantage of the proposed scheme is that it is a uniform operation mode that can be applied over the whole line cycle. Therefore, mode transitions which are necessary for the T-type inverter in TCM operation [21] can be avoided and the quality of the grid-injected current is improved.

According to Fig. 3, the inductor current slope can be expressed in (1), and the conduction times of the three stage inductor current must satisfy (2). Therefore, there are only two independent variables (T_1 and T_2) among the three conduction times of the inductor current. Fig. 7 shows the actual control of the trapezoidal inductor current, which is a mixture of digital and analog control. T_1 and T_2 are calculated in digital controller in order to precisely control the average value of the trapezoidal inductor current. And, T_3 is determined by the analog detection when the inductor current reaches the reverse boundary. So the inductor current should be sensed and the analog comparator in the digital controller is used. $I_{\rm av}$ is the average value of the

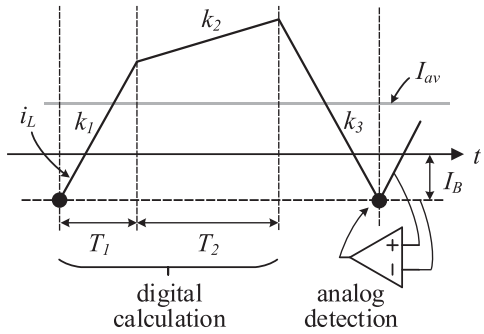

Fig. 7. Actual control of the trapezoidal inductor current.

inductor current

$$\begin{cases} k_1 = \frac{V_{\rm bus}-v_g}{L_s} \\ k_2 = \frac{V_{\rm bus}/2-v_g}{L_s} \\ k_3 = -\frac{v_g}{L_s} \end{cases} \tag{1}$$

$$T_1 \cdot k_1 + T_2 \cdot k_2 + T_3 \cdot k_3 = 0. \tag{2}$$

Since T_1 and T_2 are independent to each other, the calculation of T_1 and T_2 is complicated and may consume many computation resources in digital controllers. For simplicity, we add a constraint on T_1 and T_2, as shown in (3), where the parameter m is the proportion between T_1 and T_2. As a result, once T_1 is determined, T_2 can be calculated by

$$T_2 = m \cdot T_1 \tag{3}$$

and thereby T_1 becomes the only variable that determines the average value of the trapezoidal inductor current.

The expression for T_1 can be derived based on (1)–(3). According to Fig. 7, the average value ($I_{\rm av}$) of the trapezoidal inductor current is given in (4). By solving this equation, the expression for T_1 is derived, as shown in (5). This is a key equation for the trapezoidal wave control method. In fact, based on the constraint by (3), the derived expression for T_1 is simple and easy to be computed in digital controllers

$$\int_0^{T_1} (k_1 \cdot t - I_B)dt + \int_{T_1}^{T_1+T_2} [k_2 \cdot (t-T_1) + (k_1 \cdot T_1 - I_B)]dt + \int_{T_1+T_2}^{T_1+T_2+T_3} [k_3 \cdot (t-T_1-T_2) + (k_1 \cdot T_1 + k_2 \cdot T_2 - I_B)]dt = I_{av} \cdot (T_1+T_2+T_3) \tag{4}$$

$$T_1 = \frac{(4m+8) \cdot L_s \cdot (I_{av}+I_B)}{(m^2+4m+4) \cdot V_{\rm bus} - (2m^2+4m+4) \cdot v_g}. \tag{5}$$

From (5), we can see that m impacts the calculation of T_1, and from another point of view, m impacts the shape of the trapezoidal inductor current. So, attention should be paid when selecting the value of m. Fig. 8 illustrates the trapezoidal inductor current with different values of m. If m is too small, as shown in Fig. 8(a), the switching frequency reduction is not obvious. On the other hand, if m is too large, as shown in Fig. 8(b), the second

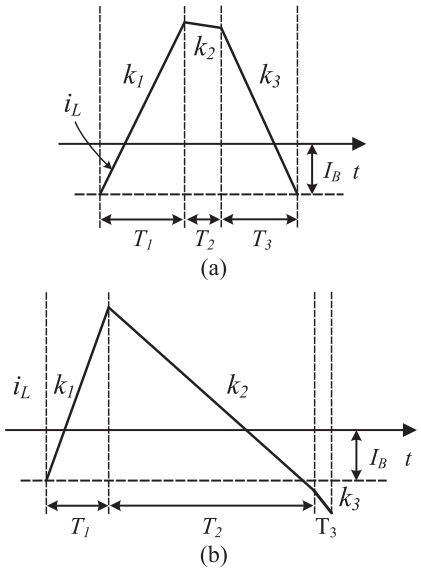

Fig. 8. Trapezoidal inductor current with different values of *m*: (a) *m* is small; (b) *m* is large.

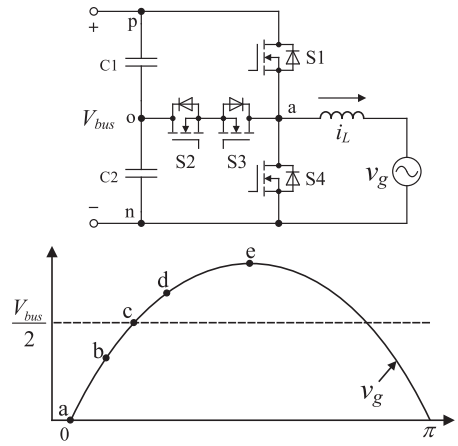

Fig. 9. Typical working points of the T-type inverter in a half line cycle.

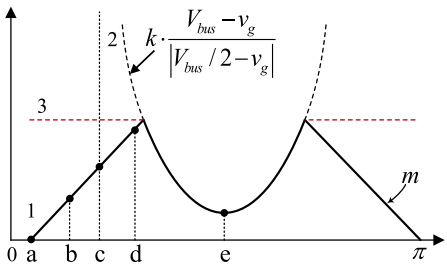

Fig. 10. Proposed value selection of m over a half line cycle.

stage of the inductor current would become too long and reach the negative boundary before entering stage 3. In order to ensure the proper operation of the trapezoidal wave control method, the second stage should be ended before the inductor current reaches the negative boundary. If the grid voltage v_g is lower than half of the bus voltage, the slope of the second stage inductor current is positive and there is no limitation for *m* theoretically. If the grid voltage v_g is higher than half of the bus voltage, the slope of the second stage inductor current becomes negative. At this time, *m* needs a limitation. The limitation can be described by (6). Rearranging (6), the maximum upper limit for *m* is obtained in (7), by which the inductor current at the end of stage 2 hits the reverse boundary exactly

$$|T_2 \cdot k_2| < |T_1 \cdot k_1| \tag{6}$$

$$m < \frac{V_{\text{bus}} - v_g}{|V_{\text{bus}}/2 - v_g|}. \tag{7}$$

III. Strategy for the Value Selection of the Proportion Between Two Conduction Times

Section II discusses the principle of the proposed trapezoidal wave control method. As mentioned above, the added constraint on the proportion (*m*) between T_1 and T_2 simplifies the calculation of the conduction time. Proportion *m* impacts the shape of the trapezoidal inductor current and its selection is flexible, whereas (7) only gives the upper limit for *m*. Therefore, this section proposes a strategy for the value selection of *m*, in order to shape the trapezoidal waveform over the whole line cycle.

Fig. 9 shows some typical working points of the T-type inverter in a half line cycle. Point c is a critical point where the grid voltage equals half of the bus voltage. At this point, the slope of the second stage inductor current equals 0. Before point c, the slope of the second stage inductor current is positive, such as point a and b. So, in this region, *m* has no upper limit theoretically. After point c, the slope of the second stage inductor current is negative, such as point d and e. In this region, if *m* is too large, the second stage of the inductor current would become too long and hit the negative boundary before entering stage 3, as shown in Fig. 8(b). To avoid this case, *m* requires an upper limit. Equation (7) gives the maximum upper limit for *m*, and a margin should be added in practical applications. Equation (8) means that the current variation of the second stage inductor current equals *k* times of the first stage inductor current. It is obvious that, in order to avoid the second stage inductor current hits the reverse boundary, *k* should be less than 1. Based on (8), (9) gives a reference value for *m* such as

$$|T_2 \cdot k_2| = k \cdot |T_1 \cdot k_1|, 0 < k < 1 \tag{8}$$

$$m = k \cdot \frac{V_{\text{bus}} - v_g}{|V_{\text{bus}}/2 - v_g|}, 0 < k < 1 \tag{9}$$

Fig. 10 shows the proposed value selection of *m* over a half line cycle. The value of *m* consists of two curves. Curve 1 starts with the zero-crossing point of the grid voltage and *m* rises linearly from zero. Curve 2 is determined by (9). Curves 1 and 2 intersect with each other and form a complete value curve for *m*. The slope of curve 1 is determined by designers, and it should not be too small. Otherwise, the proportion of the second stage inductor current becomes too small and the switching frequency

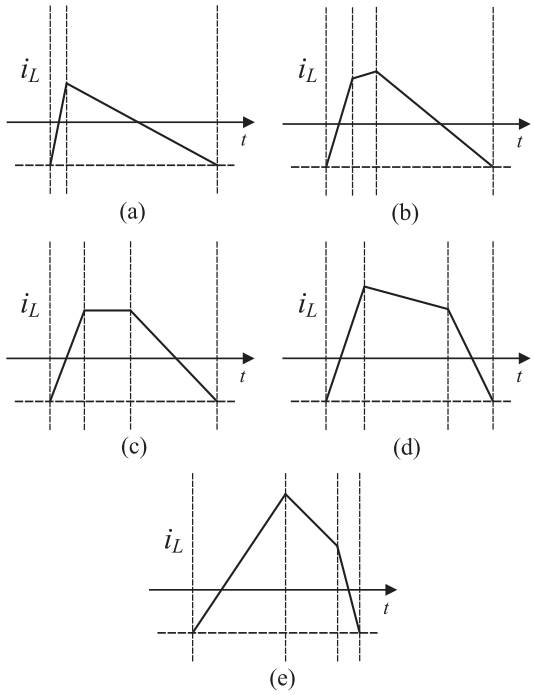

Fig. 11. Inductor current waveforms at typical working points. (a) Point a. (b) Point b. (c) Point c. (d) Point d. (e) Point e.

reduction effect is limited. The maximum of m is recommended to be no greater than 5–7.

Fig. 11 shows the inductor current waveforms at typical working points. At point a, m equals 0 and the second stage inductor current is lacking, so the trapezoidal wave degrades into triangular wave. At point b, m rises linearly and the second stage inductor current appears and increases gradually. Point c is a critical point, where the grid voltage equals half of the bus voltage, and the slope of the second stage inductor current is zero. As it comes to point d, the value of m is still obtained from curve 1, so the proportion of the second stage inductor current increases continually while the current slope becomes negative. Finally at point e, the value of m is obtained from curve 2 and is reduced largely, so the proportion of the second stage inductor current decreases accordingly.

It is worthy to mention that m gradually increases from zero as curve 1 shown in Fig. 10. If m keeps constant when grid voltage is low as curve 3 instead of curve 1 for example, the switching frequency reduction of the trapezoidal wave will be more obvious; however, the inductor current around zero-crossing points of the grid voltage would become distorted. Fig. 12 illustrates this issue.

Fig. 12(a) is the case where the inductor current is not distorted. In this case, the inductor current is positive at the end of the first stage (point 1) and flows through S1. Then, S1 is turned OFF and the current flows through the channel of S2 and the body diode of S3 (point 2). After the dead time, S3 is turned ON and the current continues to flow through the middle branch (point 3). Apparently, the change of the inductor current is consistent with the switch signals.

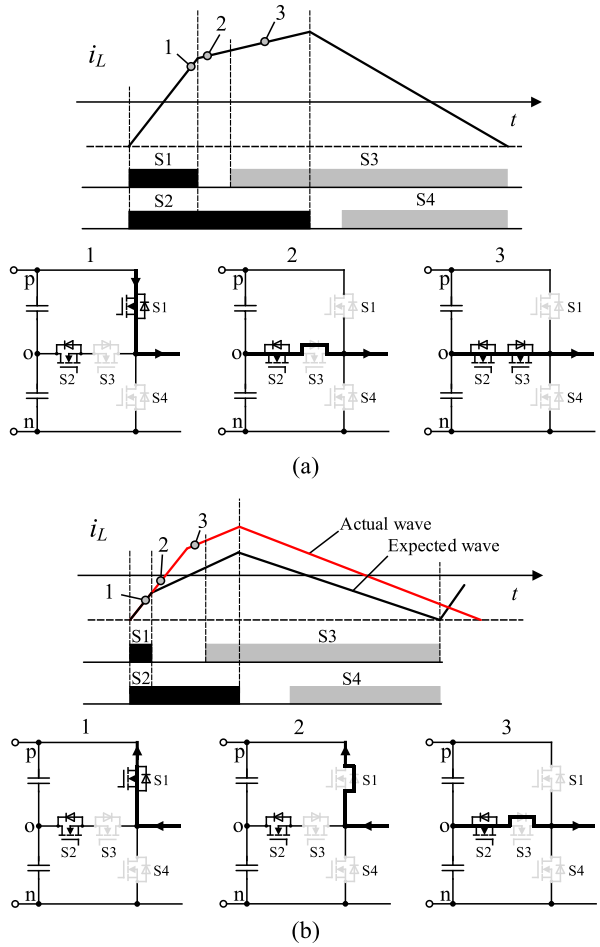

Fig. 12. Illustration about the issue of distorted inductor current. (a) Inductor current is not distorted. (b) Inductor current is distorted.

Fig. 12(b) is the case where the inductor current is distorted. In this case, the inductor current keeps negative at the end of the first stage (point 1). After that, S1 is turned OFF and the current should flow through the middle branch (S2 and S3) as expected. However, due to the existence of the dead time, S3 is not turned ON yet. So the current will still flow through the body diode of S1 in the dead time (point 2), and S3 withstands half of the bus voltage. The slew rate of the current will not be changed immediately after zero-crossing point because of the reverse recovery of the body diode of S1. During the reverse recovery, S1 is still conductive and S3 withstands half of the bus voltage. When the reverse recovery ends, S1 is capable to withstand voltage and the current starts to flow through the body diode of S3 (point 3). A short time later, the dead time ends and S3 is turned ON. So it is the dead time that makes the inductor current distorted. It can be seen that the change of the inductor current is not consistent with the switch signals, and the key reason is that the inductor current keeps negative at the end of the first stage.

The case shown in Fig. 12(b) is easy to occur around zero-crossing points of the grid voltage, especially when m is large. This is because the average inductor current is small around the zero-crossing points, and if m is large in this situation, the first

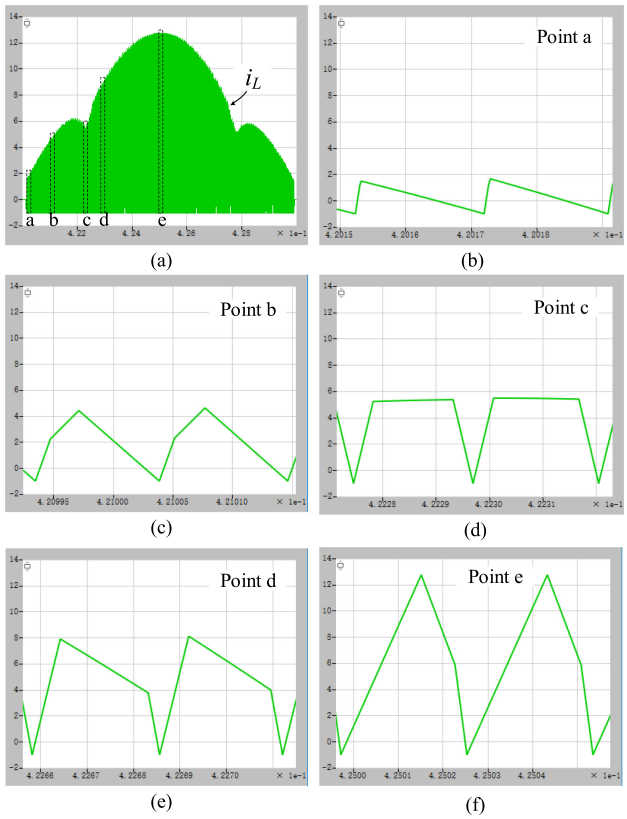

Fig. 13. Simulation results for the proposed trapezoidal wave control method. (a) Inductor current in a half line cycle. (b) Zoom-in waveform at point a. (c) Zoom-in waveform at point b. (d) Zoom-in waveform at point c. (e) Zoom-in waveform at point d. (f) Zoom-in waveform at point e.

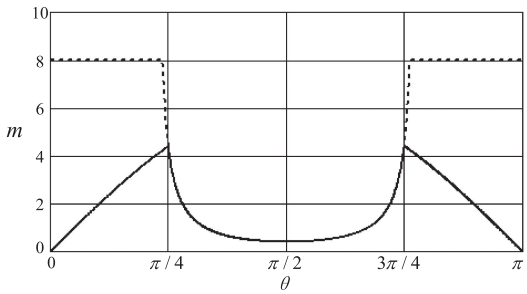

Fig. 14. Value selection curve for m in simulation.

stage of the inductor current would occupy a small proportion of the whole switching cycle and the inductor current would keep negative at the end of stage 1. This would lead to distorted current as discussed above. Therefore, curve 1 is used instead of curve 3 in Fig. 10.

Based on above analysis, Fig. 13 shows the simulation results for the proposed trapezoidal wave control method. The circuit parameters are listed as follows: dc bus voltage is 400 Vdc, grid voltage is 220 Vrms, inductor is 120 μH, and the negative current boundary is -1A. Fig. 14 shows the value selection curve for m in simulation, where the ramp curve equals $6\times\sin(\theta)$ and the k, in (8), equals 0.5.

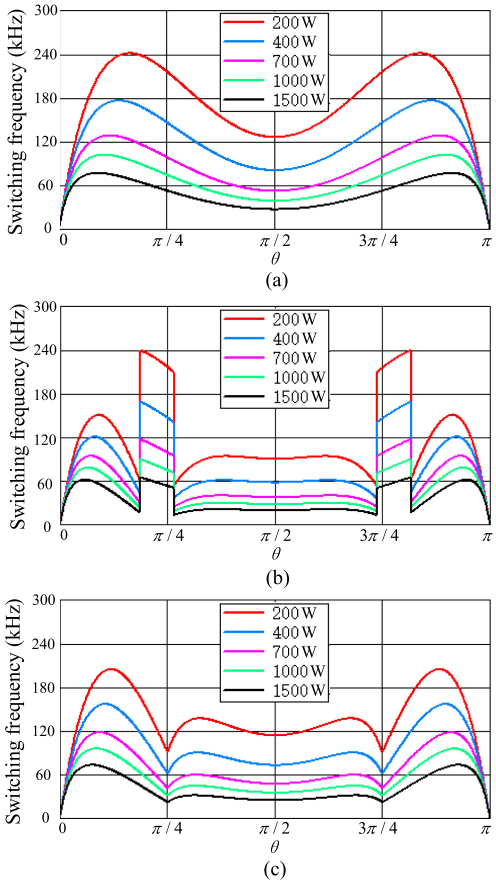

Fig. 15. Switching frequency in three types of inverters. (a) Full-bridge inverter in TCM operation. (b) T-type inverter in TCM operation. (c) T-type inverter with the proposed trapezoidal wave control method.

Fig. 15 shows the switching frequency variation in half line cycle for three types of inverters. They have the same circuit parameters and all operate in hybrid mode, which means one switching leg operates at high frequency and the other switching leg operates at line frequency. Fig. 15(a) is the switching frequency of a full-bridge inverter in TCM operation. This is a fundamental application of the TCM operation on inverters. Soft switching is achieved and the switching frequency range is large, which usually has poor light load efficiency. Fig. 15(b) is the switching frequency of a hybrid-bridge T-type inverter in TCM operation [21]. By introducing multivoltage levels, the switching frequency and related losses are reduced and the light load efficiency is improved compared with the full-bridge inverter in TCM operation. However, the switching frequency range is still high and mode transitions would deteriorate the quality of the grid-injected current. Fig. 15(c) is the switching frequency of a hybrid-bridge T-type inverter with the proposed trapezoidal wave control method. The switching frequency range is narrowed. This is good for efficiency and output current quality improvement.

IV. Prototype Design and Experimental Results

A single-phase hybrid-bridge T-type inverter has been built to verify the proposed trapezoidal wave control method. Fig. 16

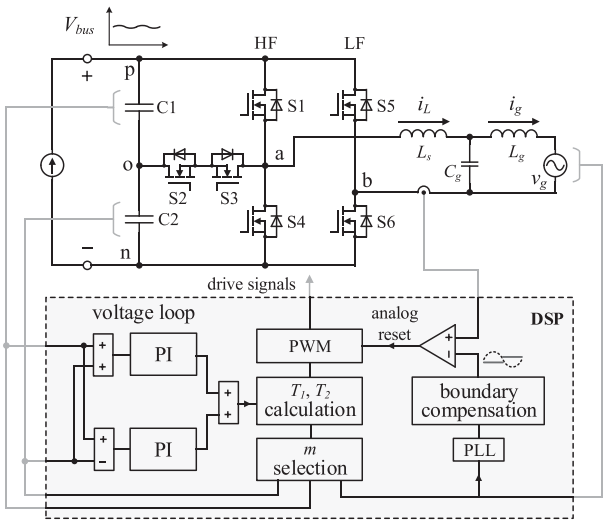

Fig. 16. Control diagram of the prototype.

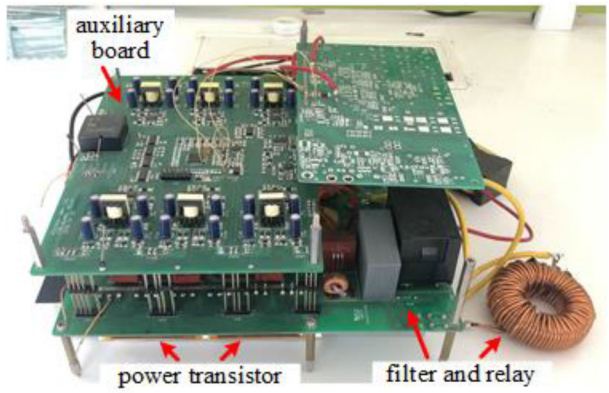

Fig. 17. Experimental prototype.

TABLE I
PROTOTYPE PARAMETERS

Parameters	Symbol	Value
Input bus voltage	V_{bus}	400Vdc
Output ac voltage	V_g	220Vrms
Rated power	P_{rated}	1000W
Inverter-side inductor	L_s	120μH
Filter capacitor	C_g	2μF
Grid-side inductor	L_g	200μH
Curve 1 in Fig. 10		6*sin(θ)
k in Fig. 10		0.3
Reverse boundary	I_B	2A
Transistors	\	IPW60R037CSFD
Hall chip	\	ACS730KLCTR-20AB-T
DSP	\	TMS320F28035

shows the control diagram of the prototype. The input of the prototype is operated as a current source, which represents maximum power point tracking (MPPT) in photovoltaic systems. The inverter is connected with the grid through an LCL filter (L_s, C_g, and L_g). There is only one voltage control loop and the grid-injected current control is open loop, so the issue of control stability does not exist. The voltage control loop is consisted of sum loop and difference loop. The sum loop regulates the input bus voltage to a given value, and the difference loop balances the voltage of the dividing capacitors. Based on the current command and the sampled value of input voltage and grid voltage, the conduction times (T_1 and T_2) of the trapezoidal wave are calculated in digital controller. All the programs run in a 25 kHz timed interrupt, which ensures enough calculation resources. The inverter-side inductor current is sensed by a hall chip with high bandwidth and low offset. The sensed signal is delivered to a built-in analog comparator in DSP controller and compared with the preset reverse boundary, so as to start a new switching cycle. The reverse inductor current is used to achieve soft switching of the switches during the dead time. So, there is a minimum threshold for the reverse current. The minimum value is related to the capacitance of the output capacitor of transistors. Obviously, the larger the capacitance, the larger the reverse current should be. On the other hand, a large reverse boundary would lead to a large peak current, which may increase the conduction loss. So the selection of the reverse boundary should be as small as possible to discharge the output capacitor during the dead time. In the prototype, the reverse boundary is set to 2 A.

When the grid voltage is close to zero, the slope of the inductor current is too small and the switching frequency will be very low. In this article, a dead zone (about 400 μs) is added during the grid-voltage zero-crossing points, where all transistors in the T-type leg are turned off. The experimental results show that the dead zone has little impact on the grid-injected current.

Fig. 17 is the photograph of the prototype and its parameters are listed in Table I. Besides the proposed scheme, the other two topologies with related control methods are also implemented with the same hardware for comparison. One is the full-bridge inverter in TCM operation and the other is the hybrid-bridge T-type inverter in TCM operation [21]. For the three types of inverters, Figs. 18–20 show the detailed inductor current waveform. Fig. 21 shows the inductor current and the grid-injected current. Table II gives the THD of the grid-injected current. Fig. 22 shows the measured efficiency. The comparison of the three types of inverters is briefly discussed as follows.

The full-bridge inverter in TCM operation is the most popular one and the detailed inductor current waveform is shown in Fig. 20. Its control is the simplest and the quality of the grid-injected current is the best, as shown in Fig. 21(a) and Table II. However, its switching frequency varies in a large scale with the load. So, its efficiency is the lowest among the three inverters as shown in Fig. 22, especially at light loads.

The hybrid-bridge T-type inverter in TCM operation can be seen as an improvement of the full-bridge inverter in TCM operation, and the detailed inductor current waveform is shown in Fig. 19. Due to multilevel operation, it reduces the switching frequency and related losses. So, its efficiency is higher than the full-bridge inverter in TCM operation, as shown in Fig. 22. Its disadvantage is that there are three operation modes in a half line cycle, as shown in Fig. 19. The switching frequency and ON-time

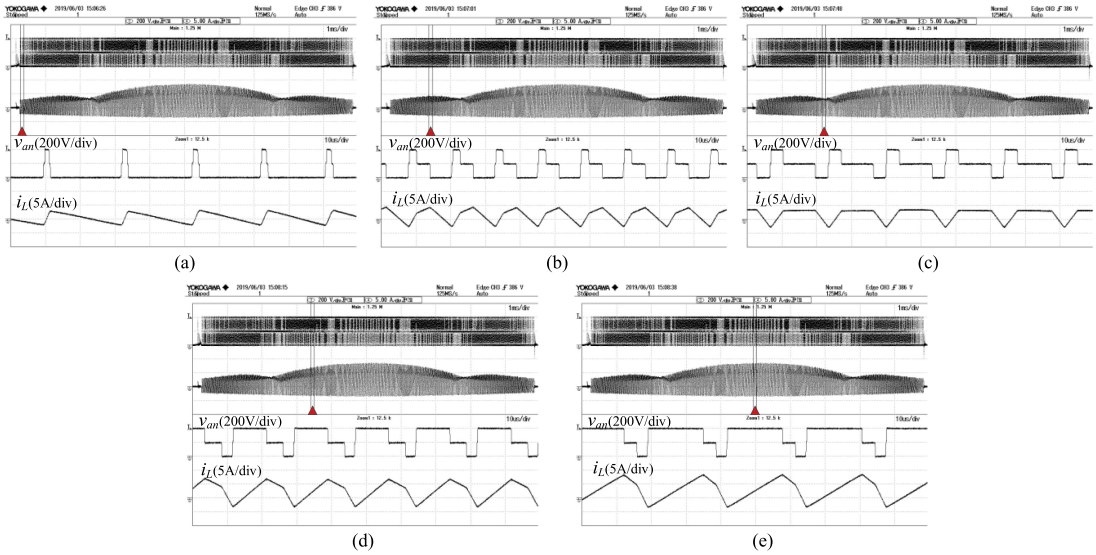

Fig. 18. Detailed inductor current waveform for the proposed trapezoidal wave control method.

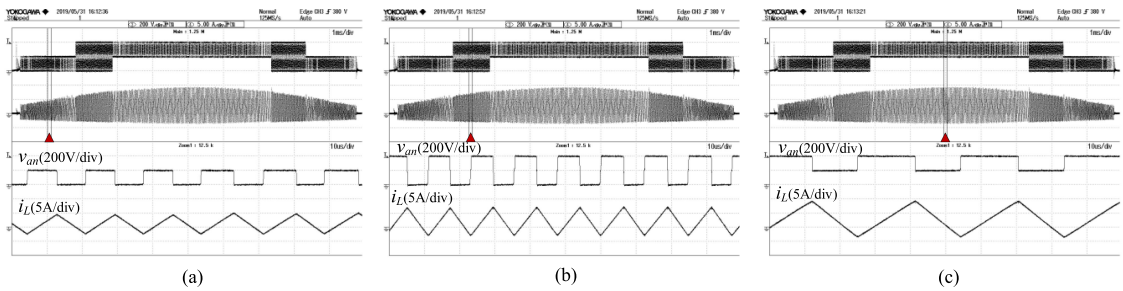

Fig. 19. Detailed inductor current waveform for the hybrid-bridge T-type inverter in TCM operation [21].

TABLE II
THD OF THE GRID-INJECTED CURRENT OF THE THREE TYPES OF INVERTERS

	400W	500W	600W	700W	800W	900W	1000W
Full-bridge inverter in TCM operation	4.0%	3.5%	2.0%	2.5%	2.5%	2.3%	3.0%
T-type inverter in TCM operation	4.5%	2.8%	3.2%	3.6%	4.0%	4.8%	5.2%
T-type inverter in trapezoidal operation	2.5%	2.0%	2.4%	3.1%	3.5%	3.8%	4.2%

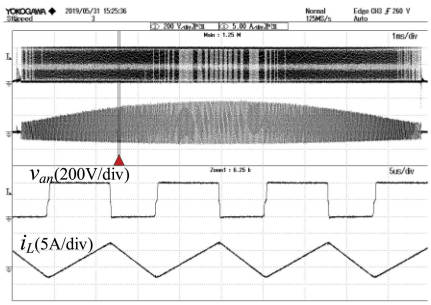

Fig. 20. Detailed inductor current waveform for the full-bridge inverter in TCM operation.

calculation are different for the three operation modes. So the average inductor current control is not very smooth during mode transitions. As a result, the quality of the grid-injected current is deteriorated. This can be seen in Fig. 21(b) that the grid-injected current is disturbed when mode transition occurs.

The hybrid-bridge T-type inverter with the proposed trapezoidal wave control method improves the conversion efficiency and the THD of the grid-injected current. According to Table II, the THD of the grid-injected current with the proposed scheme is 1% better than that of the hybrid-bridge T-type inverter in TCM operation. This is because the mode transitions are avoided and the control of the inductor current is more consistent over a half line cycle. On the other hand, the THD of the grid-injected current with the proposed scheme is not as good as that in full-bridge inverter in TCM operation. The reason is mainly caused by the inevitable delay existing in the circuit, which includes control signal propagation delay, turn-ON delay, and turn-OFF delay. The delay would slightly derivate the actual

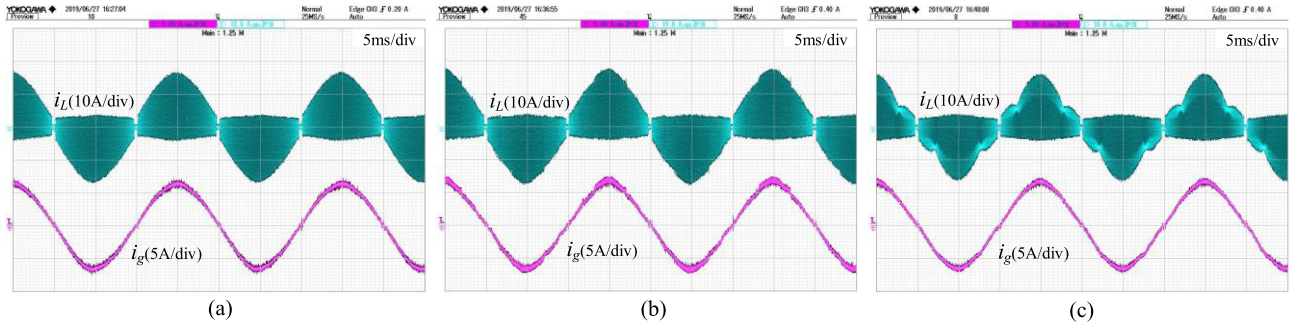

Fig. 21. Inductor current and grid-injected current of the three types of inverters. (a) Full-bridge inverter in TCM operation. (b) T-type inverter in TCM operation. (c) T-type inverter with the proposed trapezoidal wave control method.

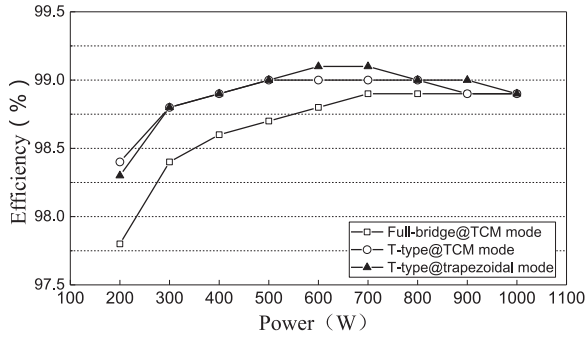

Fig. 22. Measured efficiency of the three types of inverters.

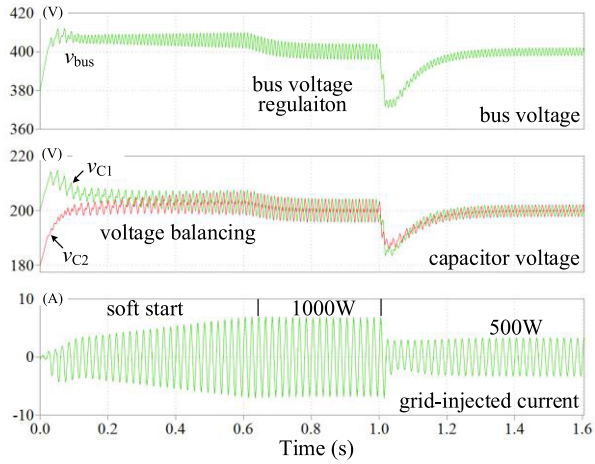

Fig. 23. Dynamic response of the proposed method with closed-loop controller in simulation.

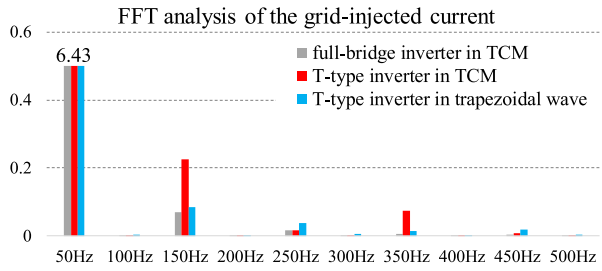

Fig. 24. FFT analysis of the grid-injected current in simulation (1 kW).

average inductor current from its desired value and thus deteriorate the output current quality. Unfortunately, the impact of the delay in the proposed scheme is greater than that in full-bridge inverter with TCM operation. For the full-bridge inverter in TCM operation, the circuit only switches once in a switching cycle. The impact of the delay is consistent over a half line cycle. For the hybrid-bridge T-type inverter with the trapezoidal operation, the circuit switches twice in a switching cycle. Therefore, the accumulation and impact of the delay time will be greater.

According to Fig. 22, the efficiency of the proposed scheme is higher than that of the full-bridge inverter in TCM operation, and is almost same as that of the T-type inverter in TCM operation. This is because the proposed scheme has a similar switching frequency reduction effect compared with the T-type inverter in TCM operation.

Fig. 23 shows the dynamic response of the proposed method in simulation. The results verify the soft start, the regulation of the bus voltage, the voltage balancing of the dividing capacitors, and the transient process caused by sudden load change.

Fig. 24 shows the FFT analysis of the grid-injected current in simulation at 1 kW. The electrical parameters are the same with Table I. Compared with the T-type inverter in TCM, the proposed method has lower third- and seventh-order harmonics. This is mainly related to the elimination of mode transitions of the T-type inverter in TCM. In a line cycle, the T-type inverter in TCM has mode transitions (three-level and two-level), even though the average current is the same (theoretically). The switching frequency changes a lot, and this will cause filter dynamic response and parasitic oscillation, so the output current has unexpected oscillations. This is consistent with the discussion above and the measured THD in Table II.

Based on above analysis, Fig. 25 illustrates the performance comparison among the three types of inverters. In addition, the proposed scheme is more balanced in efficiency and the grid-injected current quality.

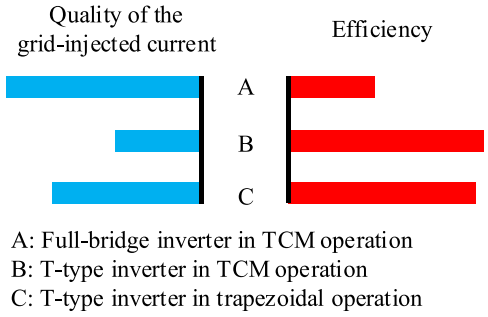

Fig. 25. Performance comparison among the three types of inverters.

V. Conclusion

This article proposes a novel trapezoidal wave control method for a single phase grid-tied hybrid-bridge T-type inverter. The trapezoidal inductor current is divided into three stages in a switching cycle, and the conduction times of the first two stages should be calculated. In order to simplify the control and calculation, this article adds a constraint on the proportion between first two-stage inductor current and thus only one conduction time needs to be determined. This article also proposes a strategy for the value selection of the proportion between the first two-stage inductor current.

A prototype has been built to verify the proposed method. On the same prototype, three inverter operations are tested, which are full-bridge inverter in TCM operation, T-type inverter in TCM operation, and T-type inverter with the proposed method. The experimental results show that the efficiency by the proposed method is higher than the full-bridge inverter in TCM operation, and is basically the same with the T-type inverter in TCM operation. On the other hand, the proposed method improves the quality of the grid-injected current compared to the T-type inverter in TCM operation. So, the proposed method brings a comprehensive improvement in efficiency and output current quality.

References

[1] S. B. Kjaer, J. K. Pedersen, and F. Blaabjerg, "A review of single-phase grid-connected inverters for photovoltaic modules," *IEEE Trans. Ind. Appl.*, vol. 41, no. 5, pp. 1292–1306, Sep./Oct. 2005.

[2] Q. Li and P. Wolfs, "A review of the single phase photovoltaic module integrated converter topologies with three different DC link configurations," *IEEE Trans. Power Electron.*, vol. 23, no. 3, pp. 1320–1333, May 2008.

[3] M. D. Bellar, T. S. Wu, A. Tchamdjou, J. Mahdavi, and M. Ehsani, "A review of soft-switched DC-AC converters," *IEEE Trans. Ind. Appl.*, vol. 34, no. 4, pp. 847–860, Jul./Aug. 1998.

[4] R. C. Beltrame, J. R. R. Zientarski, M. L. da Silva Martins, J. R. Pinheiro, and H. L. Hey, "Simplified zero-voltage-transition circuits applied to bidirectional poles: Concept and synthesis methodology," *IEEE Trans. Power Electron.*, vol. 26, no. 6, pp. 1765–1176, Jun. 2011.

[5] Y. Li and F. C. Lee, "A generalized zero-current-transition concept to simplify multilevel ZCT converters," *IEEE Trans. Ind. Appl.*, vol. 42, no. 5, pp. 1310–1320, Sep./Oct. 2006.

[6] M. Schweizer and J. W. Kolar, "Design and implementation of a highly efficient three-level T-Type converter for low-voltage applications," *IEEE Trans. Power Electron.*, vol. 28, no. 2, pp. 899–907, Feb. 2013.

[7] I. Yoscovich, T. Glovinsky, G. Sella, and Y. Galin, "Multi-level inverter with flying capacitor topology," Pat. Application US9318974B2, 2016.

[8] R. Gonzalez, E. Gubia, J. Lopez, and L. Marroyo, "Transformerless single-phase multilevel-based photovoltaic inverter," *IEEE Trans. Ind. Electron.*, vol. 55, no. 7, pp. 2694–2702, Jul. 2008.

[9] R. Stala, "Application of balancing circuit for DC-link voltages balance in a single-phase diode-clamped inverter with two three-level legs," *IEEE Trans. Ind. Electron.*, vol. 58, no. 9, pp. 4185–4195, Sep. 2011.

[10] S.-J. Park, F.-S. Kang, M. H. Lee, and C.-U. Kim, "A new single-phase five-level PWM inverter employing a deadbeat control scheme," *IEEE Trans. Power Electron.*, vol. 18, no. 3, pp. 831–843, May 2003.

[11] W. Zhu, K. Zhou, M. Cheng, L. Zhu, and X. Su, "PWM modulated three-level single-phase grid-connected PV inverter," in *Proc. Int. Conf. Elect. Mach. Syst.*, Beijing, China, 2011, pp. 1–3.

[12] Y. Zhang and L. Sun, "An efficient control strategy for a five-level inverter comprising flying-capacitor asymmetric H-bridge," *IEEE Trans. Ind. Electron.*, vol. 58, no. 9, pp. 4000–4009, Sep. 2011.

[13] G. Buticchi, E. Lorenzani, and G. Franceschini, "A five-level single-phase grid-connected converter for renewable distributed systems," *IEEE Trans. Ind. Electron.*, vol. 60, no. 3, pp. 906–918, Mar. 2013.

[14] J. W. Kim, S. M. Choi, and K. T. Kim, "Variable on-time control of the critical conduction mode boost power factor correction converter to improve zero-crossing distortion," in *Proc. Int. Conf. Power Electron. Drives Syst.*, Kuala Lumpur, Malaysia, 2005, pp. 1542–1546.

[15] J. Biela, D. Hassler, J. Miniböck, and J. W. Kolar, "Optimal design of a 5kW/dm3 / 98.3% efficient TCM resonant transition single-phase PFC rectifier," in *Proc. Int. Power Electron. Conf.*, Sapporo, Japan, 2010, pp. 1709–1716.

[16] K. C. Juang, S. J. Chiang, and W. M. Xiao, "A grid-tied flyback-based PV inverter with BCM variable frequency voltage mode control," in *Proc. Int. Symp. Intell. Signal Process. Commun. Syst.*, New Taipei, Taiwan, 2012, pp. 598–603.

[17] M. Gao, M. Chen, C. Zhang, and Z. Qian, "Analysis and Implementation of an improved flyback inverter for photovoltaic AC module applications," *IEEE Trans. Power Electron.*, vol. 29, no. 7, pp. 3428–3444, Jul. 2014.

[18] Q. Zhang, H. Hu, D. Zhang, X. Fang, Z. J. Shen, and I. Bartarseh, "A controlled-type zvs technique without auxiliary components for the low power DC/AC inverter," *IEEE Trans. Power Electron.*, vol. 28, no. 7, pp. 3287–3296, Jul. 2013.

[19] A. Amirahmadi *et al.*, "Hybrid ZVS BCM current controlled three-phase microinverter," *IEEE Trans. Power Electron.*, vol. 29, no. 4, pp. 2124–2134, Apr. 2014.

[20] D. Leuenberger and J. Biela, "Comparison of a soft switched TCM T-Type inverter to hard switched inverters for a 3 phase PV grid interface," in *Proc. 15th Int. Power Electron. Motion Control Conf.*, Novi Sad, Serbia, 2012, pp. LS1d.1-1–LS1d.1-8.

[21] Z. Zhang, J. Zhang, S. Shao, and J. Zhang, "A high-efficiency single-phase T-Type BCM microinverter," *IEEE Trans. Power Electron.*, vol. 34, no. 1, pp. 984–995, Jan. 2019.

[22] Z. Zhang, M. Chen, M. Gao, Q. Mo, and Z. Qian, "An optimal control method for grid-connected photovoltaic micro-inverter to improve the efficiency at light-load condition," in *Proc. IEEE Energy Convers. Congr. Expo.*, Phoenix, Arizona, 2011, pp. 219–224.

[23] G. C. Christidis, A. C. Nanakos, and E. C. Tatakis, "Analysis of a flyback current source inverter under hybrid DCM-BCM operation," in *Proc. 17th Eur. Conf. Power Electron. Appl.*, Geneva, Switzerland, 2015, pp. 1–10.

[24] G. C. Christidis, A. C. Nanakos, and E. C. Tatakis, "Hybrid discontinuous/boundary conduction mode of flyback microinverter for AC–PV modules," *IEEE Trans. Power Electron.*, vol. 31, no. 6, pp. 4195–4205, Jun. 2016.

[25] T. Lodh, N. Pragallapati, and V. Agarwal, "An improved control scheme for interleaved flyback converter based micro-inverter to achieve high efficiency," in *Proc. IEEE first Int. Conf. Power Electron., Intell. Control Energy Syst.*, Delhi, India, 2016, pp. 1–6.

[26] A. Amirahmadi, L. Chen, U. Somani, H. Hu, N. Kutkut, and I. Bartarseh, "High efficiency dual-mode current modulation method for low-power DC/AC inverters," *IEEE Trans. Power Electron.*, vol. 29, no. 6, pp. 2638–2642, Jun. 2014.

[27] A. Amirahmadi, U. Somani, L. Chen, N. Kutkut, and I. Batarseh, "Variable boundary dual mode current modulation scheme for three-phase micro-inverter," in *Proc. IEEE Appl. Power Electron. Conf. Expo.*, Fort Worth, Texas, 2014, pp. 650–654.

[28] S. M. Tayebi and I. Batarseh, "Analysis and optimization of variable-frequency soft-switching peak current mode control techniques for microinverters," *IEEE Trans. Power Electron.*, vol. 33, no. 2, pp. 1644–1653, Feb. 2018.

Zhen Zhang received the B.S. degree in electrical engineering in 2013 from Zhejiang University, Hangzhou, China, where he is currently working toward the Ph.D. degree in electrical engineering.

His current research interests include control methods and topologies for high-efficiency microinverters.

Junming Zhang (Senior Member, IEEE) received the B.S., M.S., and Ph.D. degrees from Zhejiang University, Hangzhou, China, in 1996, 2000, and 2004, respectively, all in electrical engineering.

He is currently a Professor with the College of Electrical Engineering, Zhejiang University. From 2010 to 2011, he was a Visiting Scholar with the Department of Electrical and Computer Engineering, Michigan State University, East Lansing, MI, USA. His research interests include power electronics system integrations, power management, and high-efficiency converters.

Shuai Shao (Member, IEEE) received the B.S. degree from Zhejiang University, China, in 2010, and the Ph.D. degree in electrical and electronic engineering from the University of Nottingham, U.K., in 2015.

In 2015, he was a Lecturer with the College of Electrical Engineering, Zhejiang University, where he was promoted to an Associate Professor in 2020. He has authored more than 30 peer-reviewed technical papers. His research interests include solid-state transformers, bidirectional dc–dc converters, and fault detection in power converters.

Dr. Shao currently serves as a Guest Associated Editor of IEEE JOURNAL OF EMERGING AND SELECTED TOPICS IN POWER ELECTRONICS.